Time-Domain Measurement of the Electromagnetic Properties of Materials

Clifton Carthelle Courtney, *Member, IEEE*

***Abstract*— A time-domain measurement and data-reduction technique is presented that can yield the broad-band frequency-dependent values of a sample material's electrical properties (complex permittivity and permeability). The method uses the material's response to the spectral content of a fast rise-time pulse to determine the frequency dependence of the complex relative permittivity (ε_r) and permeability (μ_r). The measurement procedure and data-reduction scheme are described, and the derived material values for a sample material are given. The advantages of this method include a potentially lower equipment cost and the avoidance of awkward calibration procedures that are inherent in frequency-domain methods. Though the material examined was nonmagnetic, the procedure is general and rigorous (for low-loss materials, low dispersion over the bandwidth) for the determination of both electrical and magnetic properties.**

***Index Terms*— Bounce diagram, coaxial line, complex permeability, complex permittivity, Fourier transform, s-parameters, time domain, wave propagation, wide band.**

I. Introduction

A MICROWAVE analysis or design application often requires accurate knowledge of a material's complex relative permittivity ($\varepsilon_r = \varepsilon_r' - j\varepsilon_r''$) and permeability ($\mu_r = \mu_r' - j\mu_r''$). For example, knowledge of the frequency dependence of ε_r and μ_r is required for the design of radar-absorbing structures and microwave transmission lines, and simulation and analysis of the propagation of electromagnetic waves in and through complex media. Frequency-domain techniques to measure material properties are well known and include lumped-circuit and balanced-bridge methods at low frequencies. TEM transmission line, waveguide, and resonant cavity schemes [1] are often used at higher frequencies. A comprehensive overview of measurement techniques to determine a material's electromagnetic properties can be found in [2]. This paper describes a time-domain measurement technique that can yield the complex electrical and magnetic properties of a sample material. The advantages of this method include a potentially lower equipment cost and the avoidance of awkward calibration procedures that are inherent in frequency-domain methods.

In the late 1960's and early 1970's, before the advent of the automatic network analyzer, time-domain methods were popular [3], [4]. These techniques used a material's response to the spectral content of a fast rise-time pulse to determine the frequency dependence of the complex relative permittivity (ε_r) and permeability (μ_r). However, the method described in [4] relied upon approximations that may not be valid for some cases of interest. In [4], the data-reduction method used the first components of the reflected and transmitted waveforms and ignored the infinitely many bounces that one would observe in the time domain. The processing procedure presented in this paper completely accounts for all components of the reflected and transmitted waveforms and eliminates some of the approximations and sources of potential error of the earlier work.

The paper is organized as follows. Section II provides a brief review of the theory of time–harmonic TEM propagation in a transmission line, s-parameters, and a procedure to determine the material's electrical properties from a pair of associated s-parameters. Section III describes how s-parameters are determined from time-domain measurements of an incident and partial components of the reflected and transmitted waveforms. Finally, Section IV presents the measured frequency dependence of the complex relative permittivity (ε_r) and permeability (μ_r) of a common material.

II. Transmission-Line s-Parameters and Determination of Material Electromagnetic Parameters

TEM wave propagation in a sample-loaded coaxial transmission line and the relationships of the microwave time–harmonic s-parameters (s_{11} and s_{21}) to the transmission-line properties are described in this section. Also, an algorithm for extracting complex ε_r and μ_r from knowledge of the scattering parameters is reviewed.

A. Time–Harmonic TEM Propagation in a Two-Media Region

Consider the situation shown in Fig. 1, which depicts a TEM wave that propagates on a coaxial transmission line and is incident on an interface between Region 1 (ε_0, μ_0) and Region 2 (ε_2, μ_2). A second interface between Regions 2 and 3 (ε_0, μ_0) is also indicated. Shown as well is the length, one-way propagation time, and propagation constant of each region. For observation locations in Regions 1 and 3, the signals of interest include E^{inc}, E^{ref} = the total reflected waveform in Region 1, and E^{tran} = the total transmitted waveform in Region 3. In the following, uppercase signal names denote time–harmonic quantities, which are functions of frequency, while lowercase signal names indicate signals, which are functions of time. Also, to minimize the number of variable names, we will denote a signal as unprimed if it is referenced to the location at the tip of the arrow in Fig. 1, and primed if it is referenced to the location at the base of

Manuscript received December 30, 1996; revised February 13, 1998. This work was supported by the Phillips Laboratory, Kirtland Air Force Base, NM, under Contract F29601-93-C-0200.

The author is with Voss Scientific, Albuquerque, NM 87108 USA.

Publisher Item Identifier S 0018-9480(98)03159-7.

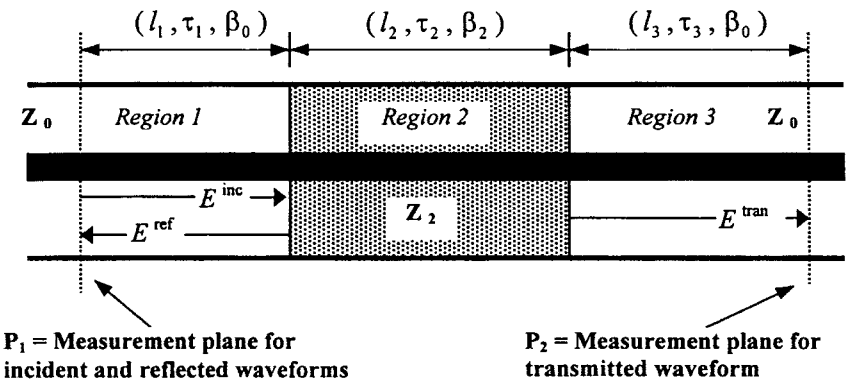

Fig. 1. A diagram of the coaxial transmission line that holds the sample material is shown. The measurement locations are indicated, and the length, one-way time of flight, and propagation constant for each region are indicated.

the arrow. The usual microwave s-parameters, referenced to the P_1 and P_2 measurement locations, can be written for time–harmonic excitation as

$$s'_{11}(\omega) = \frac{E^{\text{ref}}}{E'^{\text{inc}}} \quad \text{and} \quad s'_{21}(\omega) = \frac{E^{\text{tran}}}{E'^{\text{inc}}}. \tag{1a}$$

These values can be referenced to the front and back sample material interfaces or

$$s_{11}(\omega) = s'_{11}(\omega)e^{+j2\beta_0 l_1}$$

and

$$s_{21}(\omega) = s'_{21}(\omega)e^{+j(\beta_0 l_1 + \beta_0 l_3)}. \tag{1b}$$

In terms of the wave impedance of each region, the s-parameters referenced to the interfaces between Regions 1 and 3 can be written as

$$s_{11}(\omega) = \frac{(Z_2^2 - Z_0^2)\cdot(1 - e^{-j2\beta_2 l_2})}{(Z_2+Z_0)^2 - (Z_2 - Z_0)^2 \cdot e^{-j2\beta_2 l_2}} \tag{2a}$$

and

$$s_{21}(\omega) = \frac{4(Z_0 Z_2)\cdot e^{-j\beta_2 l_2}}{(Z_2+Z_0)^2 - (Z_2 - Z_0)^2 \cdot e^{-j\beta_2 l_2}}. \tag{2b}$$

In the above [6], $\varepsilon_2 = \varepsilon_0 \cdot (\varepsilon'_{r2} - j\varepsilon''_{r2})$, $\mu_2 = \mu_0 \cdot (\mu'_{r2} - j\mu''_{r2})$, $Z_0 = \sqrt{\mu_0/\varepsilon_0}$, $Z_2 = \sqrt{\mu_2/\varepsilon_2}$, $\beta_0 = \omega/c_0$, and $\beta_2 = \omega\sqrt{\varepsilon_{r2}\cdot\mu_{r2}}/c_0$, where c_0 = speed of light in vacuum.

B. Frequency-Dependent Material Properties From Knowledge of s_{11} and s_{21}

Given the measured values of the s-parameters s_{11} and s_{21} associated with a specific material measured in a coaxial fixture similar to that shown in Fig. 1, one can determine the material properties ε_r and μ_r. A procedure for extracting the values is given below. It follows the algorithm presented by Nicolson and Ross [4] and summarized by Lederer [6].

Equation (2a) and (2b) can be rewritten in a more compact and convenient form as

$$s_{11}(\omega) = \frac{(1 - z^2)\cdot\Gamma_{12}}{1 - \Gamma_{12}^2 \cdot z^2} \tag{3a}$$

and

$$s_{21}(\omega) = \frac{(1 - \Gamma_{12}^2)\cdot z}{1 - \Gamma_{12}^2 \cdot z^2} \tag{3b}$$

where $\Gamma_{ab} = (Z_b - Z_a)/(Z_b + Z_a)$ = the reflection coefficient for a wave passing from the semi-infinite Region a into the semi-infinite Region b, and $z = e^{-j\beta_2 l_2}$. It can then be shown that the following relations hold:

$$\Gamma_{12} = X \pm \sqrt{X^2 - 1} \tag{4a}$$

and

$$z = \frac{s_{11} + s_{21} - \Gamma_{12}}{1 - (s_{11} + s_{21})\cdot\Gamma_{12}} \tag{4b}$$

where X is expressed in terms of the scattering parameters as

$$X = \frac{1 - (s_{21}^2 - s_{11}^2)}{2s_{11}} \pm \sqrt{\left[\frac{1 - (s_{21}^2 - s_{11}^2)}{2s_{11}}\right]^2 - 1}. \tag{4c}$$

From above, $z = e^{-j\beta_2 l_2} = e^{-j(\omega/c_0)\sqrt{\mu_{r2}\varepsilon_{r2}}\cdot l_2}$, and the logarithm of both sides yields [8]

$$\begin{aligned}\ln(x) &= \text{Ln}|z| + j\arg(z)\\ &= \text{Ln}|e^{j(\omega/c_0)\sqrt{\mu_{r2}\varepsilon_{r2}}\cdot l_2}| + j\arg[e^{-j(\omega/c_0)\sqrt{\mu_{r2}\varepsilon_{r2}}\cdot l_2}].\end{aligned} \tag{5}$$

If we assume that Region 2 is not too lossy, then

$$|z| = |e^{j(\omega/c_0)\sqrt{\mu_{r2}\varepsilon_{r2}}\cdot l_2}| \approx 1 \tag{6}$$

and

$$\ln(z) = 0 - j(\omega/c_0)\cdot\sqrt{\mu_{r2}\varepsilon_{r2}}l_2. \tag{7}$$

The product of the material parameters is available as the square of both sides of the above equation as follows:

$$\mu_{r2}\varepsilon_{r2} = -\left\{\left(\frac{c_0}{l_2\cdot\omega}\right)\cdot\ln(z)\right\}^2 = C_1. \tag{8}$$

Furthermore, $\Gamma_{12} = (Z_2 - Z_1)/(Z_2 + Z_1) = (\sqrt{\mu_{r2}/\varepsilon_{r2}} - 1)/(\sqrt{\mu_{r2}/\varepsilon_{r2}} + 1)$, and the ratio of $\mu_{r2}/\varepsilon_{r2}$ is

$$\frac{\mu_{r2}}{\varepsilon_{r2}} = \left(\frac{1+\Gamma_{12}}{1-\Gamma_{12}}\right)^2 = C_2. \tag{9}$$

With the relations expressed in (8) and (9), the material parameters can be separated as

$$\mu_{r2} = \sqrt{C_1\cdot C_2} \tag{10a}$$

and

$$\varepsilon_{r2} = \sqrt{C_1/C_2}. \tag{10b}$$

The parameters C_1 and C_2 are defined completely in terms of the s-parameters, and the material constants ε_{r2} and μ_{r2} are likewise determined.

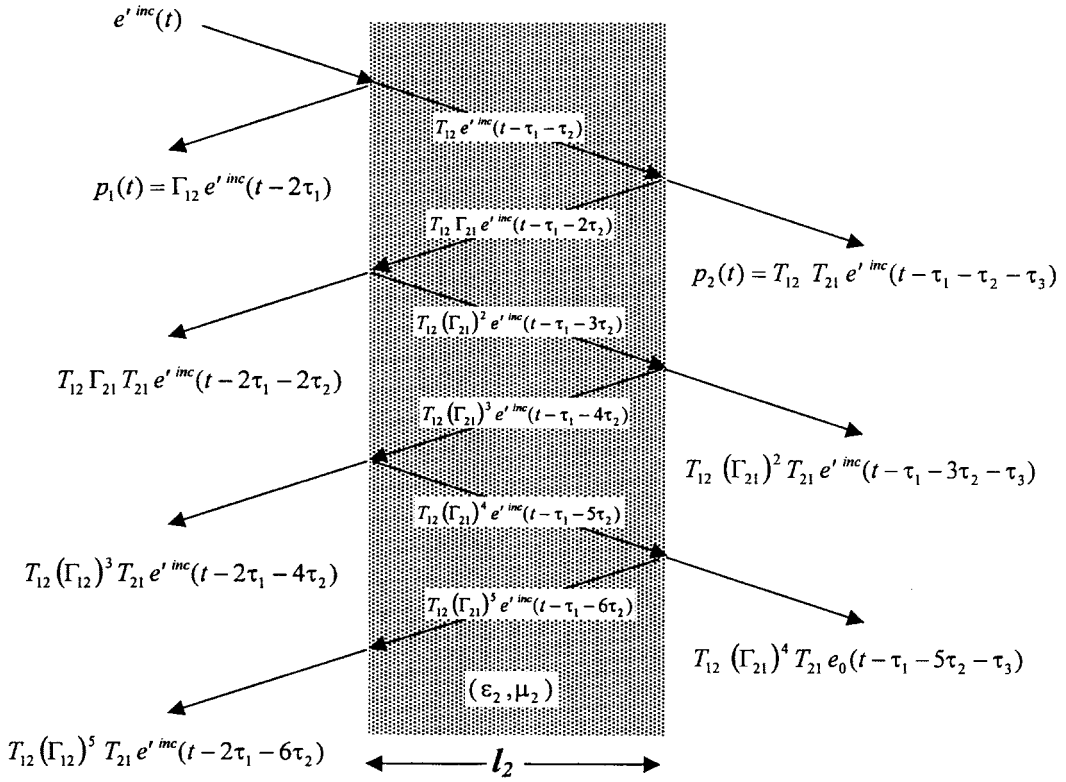

Fig. 2. A bounce diagram for the geometry depicted in Fig. 1 is shown. A transient wave undergoes an infinite number of transmissions and reflections at the interfaces of Regions 1–3.

III. Derivation of s_{11} and s_{21} From Time-Domain Measurements and Their Closed-Form Evaluation

A description of how the material parameters ε_{r2} and μ_{r2} could be determined from a complementary set of s-parameters was given in the previous section. In Section III is shown the derivation of the s-parameters from a set of transient time-domain measurements, and an explanation of how the resulting expressions can be manipulated to simplify their computation.

A. s-Parameters From Time-Domain Measurements

Consider the bounce diagram [8] shown in Fig. 2. The diagram illustrates the transient wave behavior in the coaxial transmission line of Fig. 1 if a wave $e^{\text{inc}}(t) = e'^{\text{inc}}(t-\tau_1)$ were incident on the Region 1/Region 2 interface from the left. Note that the measurement is made at position P_1 (see Fig. 1), but the waveform incident on the interface is $e^{\text{inc}}(t)$. In Fig. 2,

$$\Gamma_{12} = \frac{Z_2 - Z_0}{Z_2 + Z_0} = \text{reflection coefficient at Region 1/2 interface} \quad (11a)$$

$$\Gamma_{21} = \frac{Z_0 - Z_2}{Z_2 + Z_0} = -\Gamma_{12} = \text{reflection coefficient at Region 2/1 interface} \quad (11b)$$

$$T_{12} = 1 + \Gamma_{12} = \text{transmission coefficient at Region 1/2 interface} \quad (11c)$$

and

$$T_{21} = 1 + \Gamma_{21} = \text{transmission coefficient at Region 2/1 interface.} \quad (11d)$$

Also, τ_1 = propagation time from the point of observation in Region 1 to the Region 1/2 interface, τ_2 = propagation time across Region 2, and τ_3 = propagation time from the point of observation (position P_2) in Region 3 to the Region 2/3 interface (see Fig. 1).

The reflected (transmitted) wave is given by the convolution (*) of the incident wave with the time-domain reflection (transmission) function or

$$e'^{\text{ref}}(t) = e^{\text{inc}}(t) * s_{11}(t) = \int_0^\infty e^{\text{inc}}(\lambda) s_{11}(t-\lambda)\, d\lambda \quad (12)$$

where $e'^{\text{ref}}(t)$ is the reflected waveform at the interface of Region 1 and Region 2. In the frequency domain, this relationship becomes the following simple multiplication:

$$\begin{aligned} E^{\text{ref}}(\omega) &= E^{\text{inc}}(\omega) \cdot s_{11}(\omega) \cdot e^{-j\omega\tau_1} \\ &= E'^{\text{inc}}(\omega) \cdot s_{11}(\omega) \cdot e^{-j2\omega\tau} \end{aligned} \quad (13)$$

where the reference location is P_1, as indicated in Fig. 1. Other ways to view the time-domain interaction of the electromagnetic field with the dielectric have been presented [9], [10]. Note that although the convolution operation is implied in Fig. 2, it is not explicitly shown. Study of Fig. 2 reveals that the reflected and transmitted waves can be written as

$$\begin{aligned} e^{\text{ref}}(t) = e'^{\text{inc}}(t-2\tau_1) * \Gamma_{12} + \sum_{n=0}^{\infty} T_{21}(t) * \{(\Gamma_{21}*)^{2n+1} \\ \cdot \{T_{12} * e'^{\text{inc}}[t - 2\tau_1 - 2(n+1)\tau_2]\} \end{aligned} \quad (14a)$$

and

$$e^{\text{tran}}(t) = \{e'^{\text{inc}}(t-\tau_1-\tau_2-\tau_3) * T_{12}\} \cdot T_{21} + \sum_{n=0}^{\infty} T_{21} * \{(\Gamma_{21}*)^{2(n+)1} \cdot \{T_{12} * e'^{\text{inc}}[t-\tau_1-(3+2n)\tau_2-\tau_3]\} \quad (14b)$$

The notation $(\Gamma_{21}*)^m$ means that the expression to the right of this term is to undergo m convolutions with Γ_{21}, and the explicit time dependence is not shown. Also, for convenience and notational simplicity, the time lag in the right-hand side has been grouped together in the term $e'^{\text{inc}}(\cdot)$. Fourier transforms of both sides of (14a) and (14b) give an equivalent description in the frequency domain. That is,

$$E^{\text{ref}}(\omega) = E'^{\text{inc}}(\omega) \cdot \Gamma_{12}(\omega) \cdot e^{-j2\omega\tau_1} + \sum_{n=0}^{\infty} T_{21}(\omega) \cdot T_{12}(\omega) \cdot [\Gamma_{21}(\omega)]^{2n+1} \cdot E'^{\text{inc}}(\omega) e^{-j2\omega[\tau_1(n+1)\tau_2]} \quad (15a)$$

and

$$E^{\text{tran}}(\omega) = E'^{\text{inc}}(\omega) \cdot T_{12}(\omega) \cdot T_{21}(\omega) \cdot e^{-j\omega(\tau_1+\tau_2+\tau_3)} + \sum_{n=0}^{\infty} T_{12}(\omega) \cdot T_{21}(\omega) \cdot [\Gamma_{21}(\omega)]^{2(n+1)} \cdot E'^{\text{inc}}(\omega) \cdot e^{-j\omega[\tau_1+(3+2n)\tau_2+\tau_3]}. \quad (15b)$$

The scattering coefficients s'_{11} and s'_{21} can be expressed in the frequency domain as

$$s'_{11}(\omega) = \frac{E^{\text{ref}}(\omega)}{E'^{\text{inc}}(\omega)} = e^{-j2\omega\tau_1}\Gamma_{12}(\omega) + \sum_{n=0}^{\infty} T_{21}(\omega) \cdot T_{12}(\omega) \cdot [\Gamma_{21}(\omega)]^{2n+1} \cdot e^{-j2\omega[\tau_1+(n+1)\tau_2]} \quad (16a)$$

and

$$s'_{21}(\omega) = \frac{E^{\text{tran}}(\omega)}{E'^{\text{inc}}(\omega)} = T_{12}(\omega) \cdot T_{21}(\omega) \cdot e^{-j\omega(\tau_1+\tau_2+\tau_3)} + \sum_{n=0}^{\infty} T_{12}(\omega) \cdot T_{21}(\omega) \cdot [\Gamma_{21}(\omega)]^{2(n+1)} \cdot e^{-j\omega[\tau_1+(3+2n)\tau_2+\tau_3]}. \quad (16b)$$

The important point to note about (16a) and (16b) is that the s-parameters (referenced to the measurement planes) can be completely determined in terms of $\Gamma_{12}(\omega)$ and $T_{12}(\omega)\cdot T_{21}(\omega)$, and $\Gamma_{21}(\omega)$ can be defined in terms of $\Gamma_{12}(\omega)$ through (11b).

Referring to the bounce diagram (Fig. 2), one notes that if in the time domain the first component of the (total) reflected waveform observed in Region 1 is

$$p_1(t) = \Gamma_{12} * e'^{\text{inc}}(t-2\tau_1) \quad (17)$$

then the time-domain reflection coefficient Γ_{12} (= the reflection coefficient at the Region 1/2 interface when the width of Region 2, $l_2 \to \infty$) can be determined directly from a measurement of $p_1(t)$. Similarly, the first transmitted component observed in Region 3 is

$$p_2(t) = T_{12} * T_{21} * e'^{\text{inc}}(t-\tau_1-\tau_2-\tau_3) \quad (18)$$

and the time-domain product of the transmission coefficients $T_{ab} \cdot T_{ba}$ (where T_{ab} = the transmission coefficient from Region a to Region b when the width of Region b, $l \to \infty$) can be determined directly from a measurement of $p_2(t)$.

The values of $\Gamma_{12}(\omega)$ and $T_{12}(\omega) \cdot T_{21}(\omega)$ are found from Fourier transforms of the measured quantities $p_1(t)$ and $p_2(t)$ [(17) and (18)], and division by the transform of the incident waveform. The scattering coefficients s'_{11} and s'_{21} can then be determined from (16a) and (16b), with the coefficients s_{11} and s_{21} determined by suitable transformation. Finally, values of material ε_2 and μ_2 can be extracted in the manner described in Section II-B.

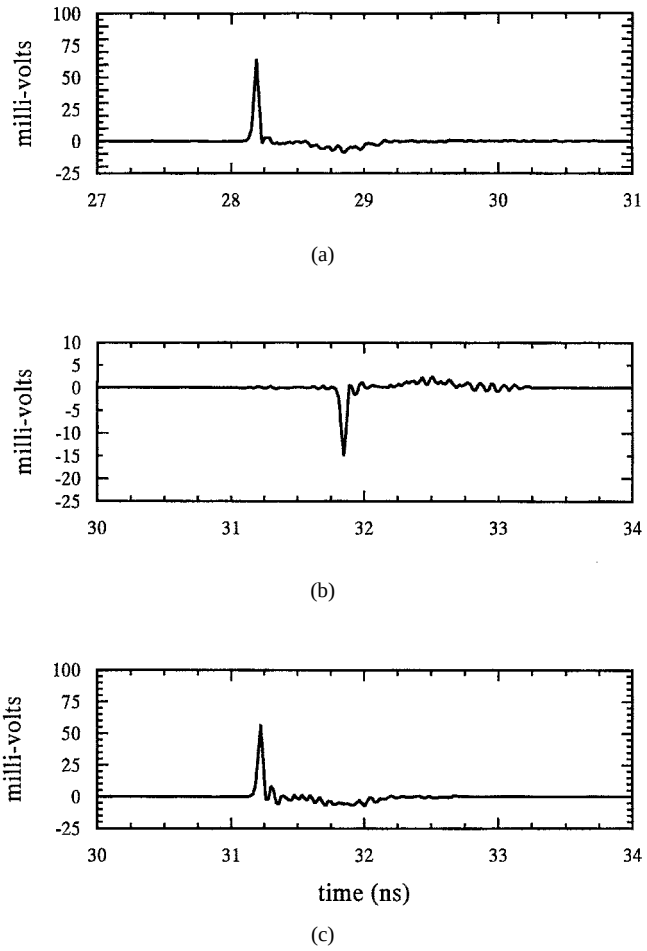

Fig. 3. The time histories of the sensor output waveforms used to construct the s-parameters and, subsequently, the material properties of the Noryl sample placed in the coaxial line are shown. (a) The time derivative of the incident pulse. (b) The time derivative of the first component of the reflected pulse. (c) The time derivative of the first component of the transmitted pulse.

B. Measurement Procedure and Simplification of the s-Parameter Expressions

To measure the material properties ε_2 and μ_2 of a sample held in a coaxial test fixture (Region 2), a voltage pulse is introduced onto the line and measured at position P_1 (see

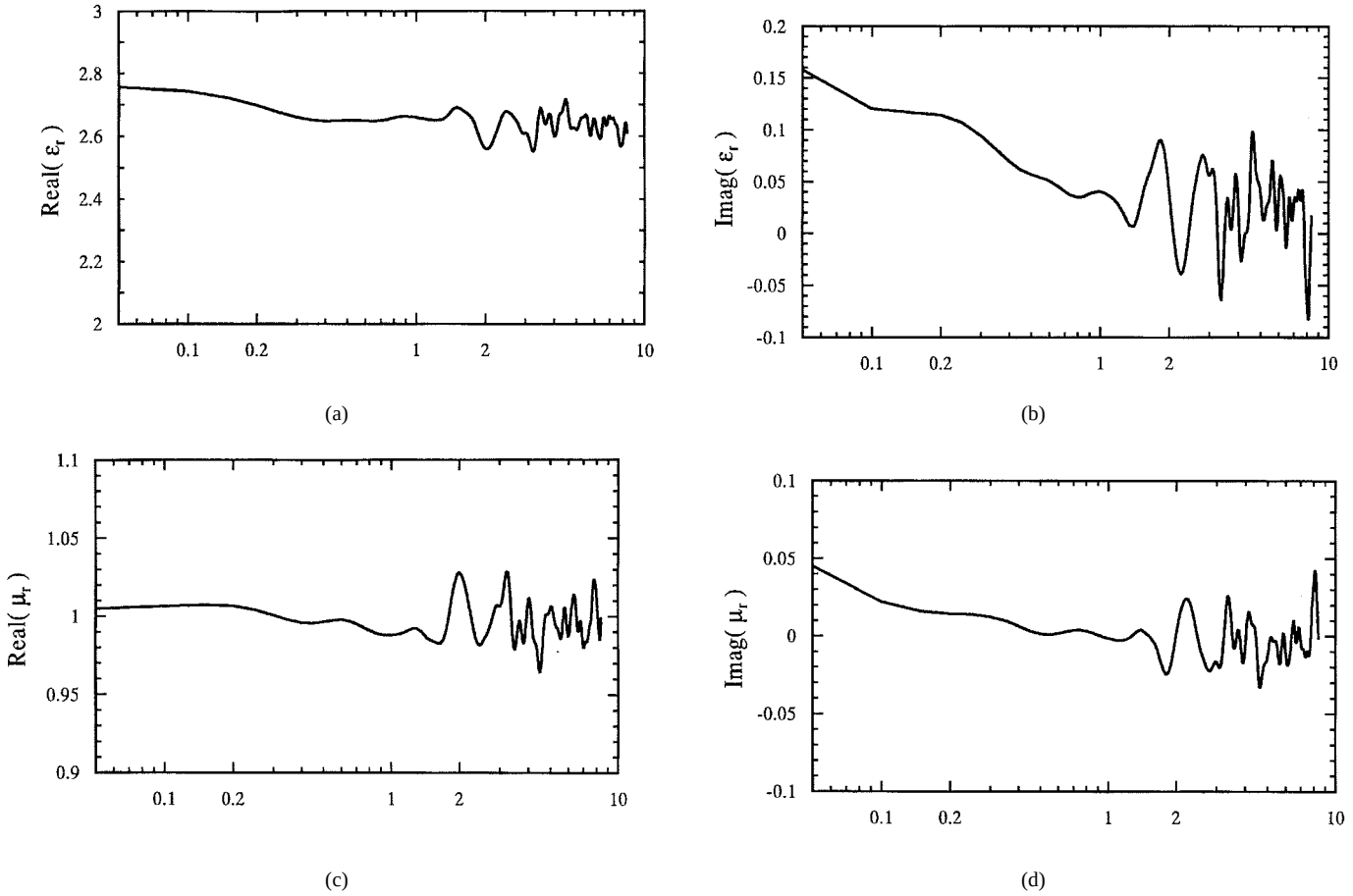

Fig. 4. Values of relative permittivity and permeability for Noryl (GE EN265) determined using the procedure described are shown. (a) The real components of values of the relative permittivity. Frequency (GHz). (b) The imaginary components of values of the relative permittivity. Frequency (GHz). (c) The real components of values of the relative permeability. Frequency (GHz). (d) The imaginary components of values of the relative permeability. Frequency (GHz).

Fig. 1). To allow uncorrupted measurement of the incident, reflected, and transmitted pulses, the incident pulsewidth must not exceed a maximum value to allow for time isolation (for this paper, τ_W = incident pulsewidth = 1 ns). The incident pulse $e^{\text{inc}}(t)$ is measured at location P_1, as is the first component of the reflected pulse $p_1(t)$. Next, the first component of the transmitted pulse $p_2(t)$ is measured at position P_2 in the coaxial test fixture. The values of τ_1, τ_2, and τ_3 are determined by overlaying the three waveforms and using a common distinguishing characteristic (e.g., waveform peak) to mark the time delays.

Once the raw data have been collected, the transforms of $p_1(t)$ and $p_2(t)$ are formed in the usual way via the Fourier transform pair

$$f(\omega) = \Im\{f(t)\} = \int_{-\infty}^{\infty} f(t) \cdot e^{-j\omega t}\, dt$$

and

$$f(t) = \Im^{-1}\{F(\omega)\} = \frac{1}{2\pi} \int_{-\infty}^{\infty} F(\omega) \cdot e^{+j\omega t}\, d\omega. \quad (19)$$

Evaluations of $\Gamma_{12}(\omega)$ and $T_{12}(\omega) \cdot T_{21}(\omega)$ via (17) and (18) are then accomplished. The next step is to form the quantities s'_{11} and s'_{21} [(16a) and (16b)]. Although originally written in terms of an infinite series, there is an easier way to evaluate the s'_{11} and s'_{21}. Consider the well-known infinite series [12]

$$\sum_{n=0}^{\infty} x^n = \frac{1}{1-x}, \qquad |x| < 1. \quad (20)$$

Equation (20) can be used to express (16a) and (16b) in forms more easily evaluated numerically. Its application allows the form of (16a) and (16b) to become

$$s'_{11}(\omega) = e^{-j2\omega\tau_1}\Gamma_{12}(\omega) + \frac{T_{21}(\omega) \cdot T_{12}(\omega) \cdot \Gamma_{21}(\omega) \cdot e^{-j2\omega(\tau_1+\tau_2)}}{1 - \Gamma_{21}(\omega)^2 \cdot e^{j2\omega\tau_2}} \quad (21a)$$

and

$$s'_{21}(\omega) = T_{12}(\omega) \cdot T_{21}(\omega) \cdot e^{j\omega(\tau_1+\tau_2+\tau_3)} + \frac{T_{12}(\omega) \cdot T_{21}(\omega) \cdot \Gamma_{21}(\omega)^2 \cdot e^{-j\omega(\tau_1+3\tau_2+\tau_3)}}{1 - \Gamma_{21}(\omega)^2 \cdot e^{-j\omega 2\tau_2}}. \quad (21b)$$

The expressions are easily evaluated from knowledge of $\Gamma_{12}(\omega)$ and $T_{12}(\omega) \cdot T_{21}(\omega)$, which are determined from measurements, Fourier transforms of $p_1(t)$ and $p_2(t)$, and simple mathematical manipulation as described above. These values are transformed to the material front and back interfaces to obtain $s_{11}(\omega)$ and $s_{21}(\omega)$, and then used to compute the values of the material parameters.

IV. Time-Domain Measurement of Noryl

A bulk sample of Noryl EN265[1] was machined to a length of 15.24 $\pm$ 0.002 54 cm (6.000 $\pm$ 0.001 in), and with cross-sectional dimensions compatible with the coaxial line test fixture (OD = 6.858 cm [2.700 in], ID = 2.9805 cm [1.173 in]). The time derivative of the incident, reflected, and transmitted waveforms was recorded. Fig. 3(a)–(c), respectively, presents the sensor output waveforms. Note that just the first components of the time derivative of the reflected and transmitted waveforms are measured. From the data shown in Fig. 3(a)–(c), the propagation time values were found to be $\tau_1 = 1.828$ ns, $\tau_2 = 0.8825$ ns, and $\tau_3 = 0.381$ ns. The reduction algorithm described earlier was exercised to form the complete response from just these partial components. The reduced values of relative complex permittivity and permeability for Noryl EN265 are given in Fig. 4(a)–(d) for the frequency range 50 MHz–8 GHz. One sees that the real part of the relative dielectric constant declines from approximately $\varepsilon_r' \approx 2.75$ at 50 MHz to approximately $\varepsilon_r' \approx 2.65$ at 1.2 GHz. The imaginary (loss) component varies from $0.01 < \varepsilon_r'' < 0.15$ over the same frequency band. Fig. 4(c) and (d) show that Noryl is a nonmagnetic material since $\mu_r' \approx 1.0$ and $\mu_r'' \approx 0.0$. To check the accuracy of the measurements given here, General Electric (GE) Corporation (a manufacturer of the material) data sheets were referenced. GE data sheets[2] give the relative dielectric constant of Noryl EN265 as 2.69 with a dissipation factor (loss tangent) as 0.0007, both at 60 Hz. These values are consistent with the results reported here.

Another interesting aspect of the data is also apparent in Fig. 4. At frequencies above 2 GHz, the results tend to oscillate about a nominal value. This behavior can be attributed to the presence of higher order propagating modes. An approximate equation for the first higher order mode allowed in a coaxial geometry [13] is

$$f^{\mathrm{TE}} = \frac{c_0}{\sqrt{\varepsilon_r}} \frac{1}{\pi(a+b)} \tag{22}$$

where the inner and outer radii are a and b, and ε_r is the dielectric constant of the material between the inner and outer conductors (the sample). Using the approximate value $\varepsilon_r \approx 3$, the first higher order mode for our fixture is allowed at $f^{\mathrm{TE}} = 1.12$ GHz and, consequently, the results above this value are less accurate because the assumption of TEM mode propagation is violated. However, the method described in this paper remains valid as long as the initial assumptions are maintained.

V. Conclusions

A measurement and data-reduction procedure to determine experimentally the complex permittivity and permeability of a material has been described. The method uses time-domain measurements of an incident and partial components of the reflected and transmitted waveforms in a coaxial transmission line that holds a sample of the material under test. The data-reduction procedure builds on the Nicolson–Ross method, but extends the procedure to account for the infinite set of reflected and transmitted waveforms. Measured values of the complex relative permittivity and permeability of Noryl, determined using the procedure described, were given. These values were compared with values of an independent source and shown to be in agreement. However, other loss mechanisms associated with the measurement (skin-effect losses, higher order modes) were not included in the analysis and the results need to be viewed in this light.

[1] Noryl EN265 manufactured by General Electric Corporation.

[2] http://www.ge.com/datasheets/NORYLEN265.html.

Acknowledgment

The author would like to thank the reviewers for the suggestions that clarified the derivations and the discussion of the experimental results.

References

[1] A. von Hippel, Ed., *Dielectric Materials and Applications*, 2nd ed. Norwood, MA: Artech House, 1995.

[2] N. Afsar, J. R. Birch, and R. N. Clarke, "The measurement of the properties of materials," *Proc. IEEE*, vol. 74, pp. 183–199, Jan. 1986.

[3] M. Nicolson and G. F. Ross, "Measurement of the intrinsic properties of materials by time-domain techniques," *IEEE Trans. Instrum. Meas.*, vol. IM-19, pp. 377–382, Nov. 1970.

[4] M. Nicolson, P. G. Mitchell, R. M. Mara, and A. M. Auckenthaler, "Time domain measurement of microwave absorbers," Air Force Avionics Lab., Air Force Syst. Command, Wright-Patterson Air Force Base, OH, Final Tech. Rep. AFAL-TR-71-353, DTIC AD-892162, Nov. 1971.

[5] R. F. Harrington, *Time–Harmonic Electromagnetic Fields.* New York: McGraw-Hill, 1961.

[6] G. Lederer, "A transmission line method for the measurement of microwave permittivity and permeability," Royal Signals and Radar Establishment, U.K., Memo. 4450, Dec. 1990.

[7] V. Churchill and J. W. Brown, *Complex Variables and Applications*, 4th ed. New York: McGraw-Hill, 1984.

[8] A. Rizzi, *Microwave Engineering: Passive Circuits.* Englewood Cliffs, NJ: Prentice-Hall, 1988.

[9] H. Cole, "Time-domain spectroscopy of dielectric materials," *IEEE Trans. Instrum. Meas.*, vol. IM-25, pp. 371–375, Dec. 1976.

[10] ——, "Evaluation of dielectric behavior by time-domain spectroscopy—I. Dielectric response by real time analysis—II. Complex permittivity," *J. Phys. Chem.*, vol. 79, no. 14, pp. 1459–1474, 1975.

[11] K. Knoop, *Infinite Sequences and Series.* New York: Dover, 1956, p. 46.

[12] D. Pozar, *Microwave Engineering.* Reading, MA: Addison-Wesley, 1993.

Clifton Carthelle Courtney (S'84–M'84) was born in Bitburg, Germany, on August 29, 1956. He received the B.S. and M.S. degrees in electrical engineering from the University of South Carolina, Columbia, in 1980 and 1984, respectively, and the Ph.D. degree in electrical engineering from Clemson University, Clemson, SC, in 1992.

Since 1992, he has been a Senior Scientist with Voss Scientific, Albuquerque, NM, where his research interests are in the areas of material characterization, antenna design and development, and microwave imaging. Previously, he was an Antenna Design Engineer with Shakespeare EFD, an electromagnetic compatibility engineer with General Electric, and was with the IIT Research Institute as an Engineer developing RF propagation models.

Dr. Courtney is a member of the IEEE Antennas and Propagation (AP), IEEE Microwave Theory and Techniques (MTT), IEEE Instrumentation and Measurement (IM), and IEEE Electromagnetic Compatibility (EMC) Societies, and is currently serving as the president of the Combined Albuquerque Chapter of the IEEE APS, MTT, and EMC Societies.